Earth and Planetary Science Letters 304 (2011) 538–546

Contents lists available at ScienceDirect

Earth and Planetary Science Letters

journal homepage: www.elsevier.com/locate/epsl

Shallow seismicity and tectonics of the central and northern Lau Basin

James A. Conder [a,*], Douglas A. Wiens [b,1]

[a] Department of Geology, Southern Illinois University, 1259 Lincoln Dr., MC 4324, Carbondale, IL, 62901, United States
[b] Department of Earth and Planetary Sciences, One Brookings Dr., Campus Box 1169, Washington University, St. Louis, MO, 63230, United States

ARTICLE INFO

Article history:
Received 1 October 2010
Received in revised form 15 February 2011
Accepted 18 February 2011

Editor: P. Shearer

Keywords:
Lau basin
crustal seismicity
backarc tectonics
T-waves

ABSTRACT

The Lau basin is an active backarc comprising several spreading centers and microplates rapidly evolving in time. As such, crustal earthquakes within the Lau Basin derive from intrabasin tectonic, volcanic, and hydrothermal sources. Because of high mantle attenuation, small earthquakes from the basin are seldom recorded on land seismographs and it has been difficult to study the pattern of crustal seismicity. However, the 1994 LABATTS ocean bottom seismograph experiment in the Lau basin recorded more than 100,000 local T- and body phases allowing for a detailed examination of basin seismotectonics. Nearly 1000 events are located within the basin proper, with another 2000 associated with the forearc and the aseismic front. We identify two previously undocumented tectonic features, a triple junction in the northwestern basin and a nanoplate in the central Lau basin. The single most seismically active feature within the Lau basin is the Lau extensional transform zone (LETZ) just north of the Central Lau Spreading Center. Significant seismicity also occurs near the northern extension of the Eastern Lau Spreading Center and along a southeast extension of the LETZ delineating the boundary of a previously unknown nanoplate. Swarm activity is common in the backarc basin and dominates regions associated with actively reorganizing tectonics. We see no evidence of deformation along the southern boundary of the Niuafo'ou microplate, where 4.5 cm/yr of strain is predicted. It is possible that the plate boundary extends eastward from the Fonualei rift (FR) tip towards the trench creating a Niuatoputapu–Tonga plate division rather than westward implied by the currently accepted Niuafo'ou–Tonga plate system, but more data are necessary from the FR to test that hypothesis. Instead, we suggest that the Niuafo'ou–Tonga pole is ~1.5° further north than previously proposed, reducing the predicted strain in this region to <2 cm/yr.

1. Introduction

The Lau backarc basin between Fiji and Tonga has been opening for the past 5–6 Ma in a wedge shaped pattern (Taylor et al., 1996). As a type example of an active backarc basin, considerable attention has been given to understanding how deformation is accommodated and distributed throughout the Lau basin (e.g., Hamburger and Isacks 1988; Isacks et al., 1968; Pelletier and Louat 1989). With a basin scale inversion of seafloor magnetization, Taylor et al. (1996) demonstrated 'typical' seafloor spreading in the backarc and showed that deformation is largely accommodated through a set of evolving microplates bounded by spreading centers and other localized boundaries. This set of boundaries forms a complex and rapidly changing system relative to other mid-ocean ridges with multiple propagating rifts and tectonically reorienting structures making up several microplates. Many of the earthquakes previously thought to indicate diffuse deformation could now be identified with tectonic boundaries and spreading centers. A three-plate kinematic model of basin opening outlines the principal mode of deformation accommodating the extension (Zellmer and Taylor, 2001 — hereafter Z&T). The three-plate model comprises the Australian plate to the west of the spreading centers, the Niuafo'ou plate positioned between the Peggy Ridge and the Fonualei rift (FR), and the Tonga plate to the south and east of the Niuafo'ou plate (Fig. 1).

This three-plate model credibly matches observed earthquake slip vector orientations and spreading rates determined by magnetic anomalies along the Lau spreading system. However, the nature of some microplate boundaries were not constrained by available geophysical observations and were either inferred or left to further study. For instance, there must be at least one microplate north of the Niuafo'ou plate, but geometry and kinematics are largely unconstrained. Also, as noted by Z&T, there is no obvious indication of where the southern boundary of the Niuafo'ou plate extends between the southern tip of the Fonualei rift and spreading system to the west (Fig. 1). Based on statistical consistency of plate boundary data (rates and azimuths), they determined that the boundary connects the Fonualei rift tip to the Central Lau Spreading Center (CLSC)–Eastern Lau Spreading Center (ELSC) overlapping discontinuity. However, despite the fact that this boundary must accommodate over 4.5 cm/yr of strain, there is no clear indication in bathymetry, seafloor

* Corresponding author. Tel.: +1 618 453 7352; fax: +1 618 453 7393.
E-mail addresses: conder@geo.siu.edu (J.A. Conder), doug@wustl.edu (D.A. Wiens).
[1] Tel.: +1 314 935 6517; fax: +1 314 935 7361.

0012-821X/$ – see front matter © 2011 Elsevier B.V. All rights reserved.
doi:10.1016/j.epsl.2011.02.032

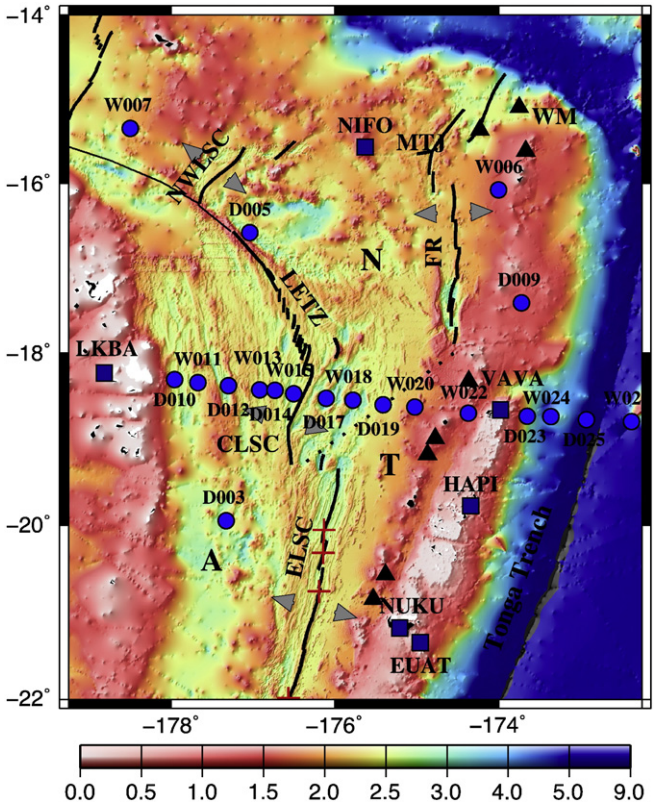

Fig. 1. Bathymetry, major tectonic features, and experiment layout in Lau basin. Color bar denotes depth in kilometers. Dark lines show well defined plate boundaries. Gray arrows show spreading directions for various spreading axes. Labels are as follows: NWLSC = Northwest Lau Spreading Center, CLSC = Central Lau Spreading Center, ELSC = Eastern Lau Spreading Center, LETZ = Lau extensional transform zone, MTJ = Mangatolu triple junction, FR = Fonualei rift, and WM = West Mata undersea volcano. Black triangles show volcanic centers active in the last couple of decades. Circles (ocean bottom) and squares (land) are seismographs used in this paper. A–N–T designations are plate geometry of Zellmer and Taylor (2001), where A = Australia, T = Tonga, and N = Niuafo'ou. Dotted line is hypothesized boundary between the Tonga and Niuafo'ou microplates.

reflectivity, seafloor magnetization, or known seismicity. It is apparent that this geologically young basin is still evolving, making some of these characteristics difficult to extract. Thus, despite the attention over the past few decades to detailing Lau backarc tectonics, there remain fundamental gaps in our understanding of the geometry and kinematics of deformation associated with Lau backarc opening.

A potentially valuable geophysical dataset that could improve our understanding of Lau microplate tectonics and intrabasin deformation is the shallow seismicity associated with accommodation of tectonic strain. Spatial patterns of crustal and uppermost mantle earthquakes can delineate localizations of active tectonic strain, while moment tensors and spatio-temporal patterns will illuminate the nature of the tectonic deformation. Previous studies relied primarily on teleseismic arrivals (e.g., Pelletier et al., 1998) and seismograph deployments on the Fijian and Tongan islands (Hamburger and Isacks, 1988). However, the unusually high seismic attenuation in the mantle beneath the basin (Roth et al., 1999) prevents seismic P and S waves from all but the largest events ($Mb \geq 4.5$) from being recorded at epicentral distances of even the nearby islands thereby restricting the amount of possible information to be gleaned regarding the frequency and distribution of seismic deformation in the basin. For example, while the 1993–1995 SPASE array, spanning a number of islands in both Fiji and Tonga (Wiens et al., 1995) produced excellent records of deep subduction events and hundreds of forearc events, only ~30 shallow basin events could be located. In contrast, a three week deployment of nine ocean bottom seismographs (OBSs) near the Peggy Ridge in 1984 detected hundreds of nearby earthquakes (Eguchi et al., 1989).

A useful phase for locating and studying shallow seismicity using OBSs is the T-phase — hydroacoustic energy traveling in the water column. T-wave energy is not susceptible to the local high crust and mantle attenuation and, T-waves also lose energy more slowly through geometrical spreading than spherically spreading body waves. As T-phases can give easily observable arrivals well beyond where body arrivals are discernible (Fig. 2), many small earthquakes may be identified that would otherwise go undetected. Hydroacoustic sensors or OBSs recording T-phases propagating in the SOFAR channel have proven able to monitor small earthquakes associated with tectonics, volcanism, and hydrothermal activity (Dziak et al., 2004; Fox et al., 2001; Smith et al., 2003).

In this paper, we examine the seismotectonics of the central and northern Lau basin using seismicity found from T and body phases recorded from the LABATTS OBS array augmented with data recorded from the simultaneously running SPASE array on the Tongan islands and the Fijian island of Lakemba (Wiens et al., 1995). Tens of thousands of clear T and body wave arrivals are used to locate microearthquakes and examine microseismic patterns to infer strain distribution within the basin. Our results demonstrate a previously undiscovered nanoplate in the central basin and a previously unknown triple junction in the northwestern basin. Further, the seismicity illuminates tectonic behavior of other microplate boundaries in both the northern and central portions of the basin.

2. Data and methods

2.1. Instrumentation and data

The ocean bottom seismograph deployment comprised thirty 4-component instruments — each having a 3-component 1 Hz sensor and differential pressure gage (Crawford et al., 2003). The OBSs recorded continuously at 32 samples per second for 3 months with about half the OBSs (marked 'W' in Fig. 1) recording at 128 Hz for the first 2 weeks for benefit of the airgunning component of the experiment. One instrument was not recovered and a few instruments failed early in the experiment (not included in Fig. 1). We also include data from six broadband land stations from the SPASE array that were simultaneously recording on the Tongan and Lau islands (Wiens et al., 1995).

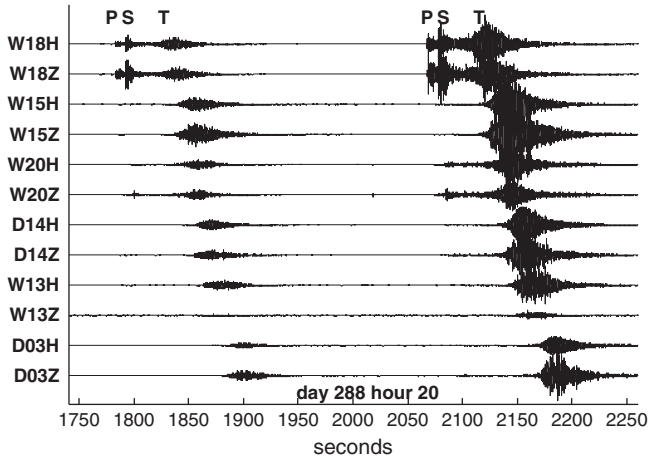

Fig. 2. Seismograms showing P, S, and T arrivals. Sesimograms are vertical and hydrophone channels for two events spaced less than 5 min apart located near the northern terminus of the ELSC. Stations are ordered by distance from epicenter. Clear body waves are only observed at the stations closest to the epicenter.

2.2. Automated arrival time determination

Hundreds to sometimes thousands of body wave and T phase arrivals are visible for each day of data recorded. To process the large number of arrivals, we do a first pass of picking arrivals via automated methods. P-waves are determined by a simple short term average-long term average (STA/LTA) algorithm applied to the vertical channel data streams. Electronic spiking is sometimes an issue, so prior to running the STA/LTA algorithm, we despike the traces using a statistical method (Hojstrup, 1993) that leaves the waveforms unchanged.

Automating arrival picks of the T-waves proves less straightforward because of the non-impulsive nature, rendering STA/LTA algorithms largely useless. Observed T-waves also tend to be high-frequency as well as non-impulsive (Fig. 2), so precise travel-time picks are somewhat ambiguous. However, because T-phases travel far more slowly than body phases, a larger error in the arrival picks can be tolerated before problematically influencing calculated hypocenter locations. To effectively automate initial T-picking, we apply a 4 Hz highpass Butterworth filter to the hydrophone records and form an envelope using a Hilbert transform of the bandpassed waveforms. To take advantage of the shape of the non-impulsive T-wave forms, we integrate a twelve second window of the resultant envelope of the hydrophone data trace. Arrivals are triggered when this integration is larger than three times the median of the corresponding envelope of an hour of the data trace. Because the T-arrivals are non-impulsive, arrival picks are assumed to be at the peak of the sliding integration of the windowed envelope.

After building the initial event and associated T-wave arrival time lists, we manually screen the picks for each event for consistency, accuracy, and the possible addition of missed P and S arrivals. P arrivals are picked as first arrivals in the 4 Hz highpassed data and S are picked on the first large excursion on the horizontals after the P arrival. The most common errors encountered in the automated picks were S-waves misattributed as P-waves and false identification of both P and T because of often noisy data. More false phase identifications could have been eliminated using a higher threshold, but at the cost of increasing false negatives. As our auto-association algorithm (grouping picks into events) is reasonably robust at elimination of false identifications but missed events cannot be remedied, we are willing to accept some false identifications. Manual screening and editing of arrival picks further tighten the resultant patterns and more than double the number of located events by improving the signal to noise ratio in the arrival time list.

2.3. Association and location

Using the arrival times, we locate each event with a standard weighted least-squares algorithm using the 1D velocity models determined across the array from airgun analysis (Crawford et al., 2003). Four different models are used depending on location of the station and/or event: Central Lau (CL), Tonga Ridge (TR), Tonga Forearc (TF), and Pacific Plate (PP) (Fig. 3). Island stations use the TR model with a 20 km thick crust. We solve for depth if eight or more body wave arrivals are identified, otherwise we fix the depth at 5 km. For the T-waves, we assume a water velocity of 1490 m/s (Dunn, 2009). Body wave travel times and derivatives are found using lookup tables generated by the TTbox routines (Knapmeyer, 2004). P, S, and T arrivals are given standard uncertainties of 1, 2, and 4 s respectively for weighting. For hypocenter-station pairs where the path traverses regions with different velocity models, we find body wave travel times and derivatives by averaging the two models.

We locate and associate events with arrival picks in a single step. After sorting picks by time, an initial pick is grouped with subsequent picks within a given time window. The time window for P is 60 s, the S window is 1.85 times the P window, and the T window is 300 s. A starting location is chosen near the station of the first pick in the group, and a best fitting location is then iterated for this group of picks using a weighted least squares scheme. Successive iterations dynamically downweight outliers to reduce their influence on the location (Willeman, 2001). If at least eight picks, including the first pick, are consistent (misfits less than the assigned standard uncertainties), those consistent picks are associated as an event. If either of these conditions are not met, no association is made and the algorithm moves to the next earliest unassociated pick and repeats the process. Because of station geometry, we test two different starting locations, one north of the first arrival station and one south and discard the one with the higher sum of squares misfit.

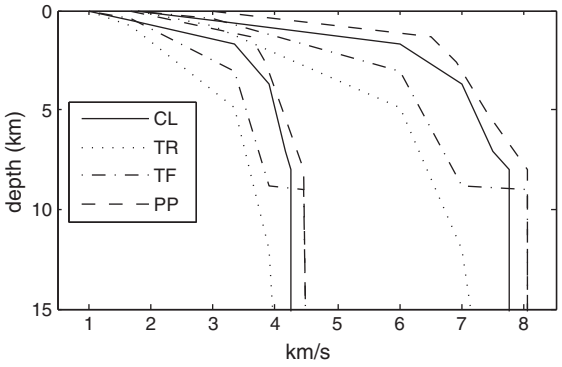

Fig. 3. P and S velocity models used for event location. Crustal velocities from Crawford et al. (2003). Four different models are CL: Central Lau, TR: Tonga ridge (island stations), TF: Tonga forearc, and PP: Pacific plate.

2.4. Event magnitudes

To get a measure of the size of the observed events, we determine a T-wave magnitudes of events with four or more associated T-waves and compare the distribution with that expected from the PDE catalog. We take the amplitude of a smoothed Hilbert envelope (Yang and Forsyth, 2003) and correct for cylindrical spreading. The assigned local scale magnitude is the log of the corrected amplitude. The distribution of events have a b-value of 1.2 while PDE basin events from 2000 to 2010 exhibit a b-value of 1.1. Adjusting the local magnitudes with a DC shift to match the expected rate from PDE suggests that the recorded events typically range in magnitude from ~2.8 to 4.5. No PDE events were recorded during the LABATTS deployment for direct comparison of waveforms, but 4.5 is a reasonable upper end as it is approaching the threshold of detection for PDE. We note that T-wave magnitudes are dependent on factors such as coupling to the seafloor, local topography, and even focal mechanism (Dziak, 2001; Park et al., 2001), so individual magnitudes have significant uncertainty to them. However, using P-waves (where four or more are available) rather than T-waves gives a similar b-value (1.1) and likely range of magnitudes.

2.5. Event clustering

Events clustered in time and location are apparent in the data. To systematically identify and examine the character of seismic event clusters, we use single-link clustering analysis (SLC) (Davis and Frohlich, 1991) applied to the resultant event catalog. SLC connects groups by making links between events that are closest to each other in some sense. All events that can be connected along a series of links smaller than a given threshold are considered a distinct cluster. SLC is especially helpful in aiding interpretation where multiple swarm signals or high degrees of background seismicity are present. For clustered seismicity, the important parameter is a coupling of space and time. For our SLC analysis, we use a time constant of 2 days/km

and a space–time distance threshold of 10 km (Davis and Frohlich, 1991).

3. Results

We locate nearly 3000 events in the backarc-arc–forearc system with about one-third of those in the backarc and two-thirds along the forearc and forearc ridge (Fig. 4). Differences between forearc and backarc seismicity are apparent with even a cursory glance. Seismicity in the forearc is more widely distributed, while seismicity in the backarc is less diffuse and more tightly restricted to plate boundaries. Backarc activity is also prone to occurring in swarms, while forearc activity exhibits negligible swarm-like behavior.

Backarc arrivals are dominated by T-waves while forearc arrivals tend to be dominated by body waves. This difference arises from a combination of factors. First, shallower hypocenters in the backarc tend to excite more hydroacoustic energy. Second, while propagation of T-waves is largely uninhibited through the backarc basin, propagation is inhibited by the forearc ridge — particularly south of Vava'u. Third, the aforementioned mantle attenuation beneath the basin tends to preclude body wave arrivals on basin stations, but there is far less attenuation beneath the forearc, so body waves are more easily observable on forearc and outer rise stations, as well as the island stations.

With the higher proportion of body waves, there is better control on depth for forearc events than in the backarc. To avoid slab seismicity, events with a confidence ellipsoid reaching the slab surface (Gudmundsson and Sambridge, 1998) or deeper are removed from this analysis. The high amount of seismicity along the forearc is not unexpected as forearcs in general exhibit deformation associated with subduction between the trench and aseismic front (Igarashi et al., 2001).

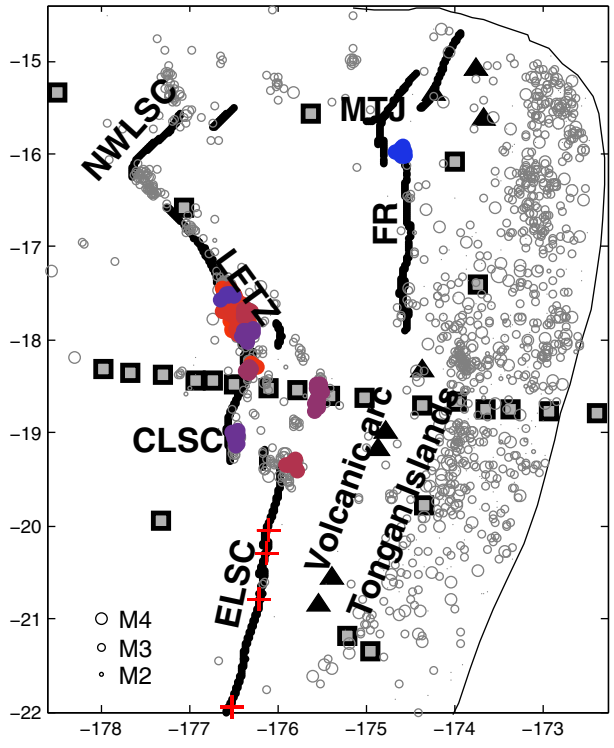

Fig. 4. Shallow basin seismicity. Epicenters found in this study west of the Tonga trench (thin black line) are shown as gray circles. Size is scaled to T magnitude adjusted to best match PDE body wave magnitudes for Lau. Magnitude scale is bottom left. Colored groups are event clusters of eight or more found by single-link-clustering analysis. Event clusters are spaced closely in both time and space. Clusters are associated with the northern termini of the Fonualei rift and Eastern Lau Spreading Center. Seven clusters are found in the LETZ, with two comprising more than seventy events each.

3.1. Location quality assessment

Uncertainties in hypocenter location are evaluated by the two sigma confidence ellipses determined by the covariance matrix of the weighted least squares formulation. Two sigma uncertainties in location are typically 5–10 km near the CLSC and ETZ and expand to 15–30 km in the extremities of the basin.

While the array was successfully designed for mantle structure and deep earthquake studies of the Tonga region (e.g., Conder and Wiens, 2006; Koper et al., 1998), the linear geometry can pose ambiguity in earthquake epicenter determination beyond formal uncertainties. Because of the geometry, most arrivals will be observed along the main line with a few arrivals registering on off-line stations. This results in off-line stations having a disproportionate data importance attached to their arrivals in the locating algorithm, meaning that erroneous picks on off-axis stations are more problematic for causing spurious locations and are also more difficult to easily discern by correlation with other stations. The biggest potential problem is that of 'mirroring' across the line as a particular location on one side of the line will fit the arrival data for the line stations just as well as a hypocenter south of the line.

To limit these problematic issues, a few different approaches are made in examination of arrival picks. Off-axis station pairs D005 with W007 and W006 with D009 are cross-checked for arrival picks where possible, but this cross-checking is limited as D009 stopped recording after 4 weeks and W007 had continual quality control problems due to electronic noise — particularly on the vertical channel. Events that appear to be deeper than a few of 10 s of kilometers (trench and subduction events) are removed when identified and when picks are too ambiguous on off-line stations to make a reasonable determination.

The CLSC ridge tip is probably the most subject to mirror problems of any tectonic feature in the basin. The mirror site for the southern segment of the CLSC is the LETZ, allowing for the possibility of leakage from the LETZ overprinting the CLSC tip. For this reason, we imposed a specific check in this region allowing only events where final locations from both starting locations were south of the line, meaning that arrivals at stations D003 and/or D005 must force the locations south of the line rather than simply allow it. As the trend of the resultant epicenters tend to follow the spreading segment rather than a SSW trend that would likely be derived from mirroring events from the ETZ, these appear to be robust, with the attached caveat.

The band of events between 18.5° and 19.5°S (CLSC to nELSC) appear to be systematically shifted eastward 5–10 km. This shift does not appear to come from any timing or location problems from the recording stations. As epicentral locations from T-waves denote where energy enters the water column, this may be an instance where nearby topographic features are acting as primary radiators rather than 'true' epicentral locations.

4. Discussion

Both spatial and temporal patterns are apparent in the seismicity. In the backarc, most events are associated with boundaries of the several microplates within the basin. Many of the patterns we see support prior work delineating tectonics of the basin (Pelletier et al., 1998; Taylor et al., 1996; Zellmer and Taylor, 2001). At the same time, the seismicity presented here provides new information that furthers and revises this prior work. A detailed examination of spatial and temporal trends in shallow basin seismicity are reported in Sections 4.1–4.3. Because of the large number of small earthquakes and the less than optimal station distribution, a few individual earthquakes may be poorly located despite their good formal uncertainties. Therefore, we focus on interpreting seismicity patterns rather than

individual isolated hypocenters. For ease of discussion, we divide the basin into northern and central portions roughly along 16°S.

4.1. Central basin

The three-plate model of Z&T applies to the basin south of ~16°S, the part with the best constrained seafloor magnetization as well as greatest coverage of bathymetry and sidescan sonar. The primary boundaries in this region include the ELSC, CLSC, FR, and PR. The three spreading centers are all propagating southward, albeit at different rates (Pelletier et al., 1998), and the PR has recently evolved from a transform fault to an extensional transform zone (Taylor et al., 1996). As well as having different strain rates and morphologies, each of these boundaries exhibits a different character in seismicity.

4.1.1. Swarm activity

While absent in the forearc, swarm activity is not unusual in the central backarc basin. Single-link clustering shows several groups associated with specific tectonic features, such as the northern terminus of the Easter Lau Spreading Center (nELSC), the extensional transform zone (ETZ) and, the northern terminus of the Fonualei rift (nFR) (Fig. 4). Only one cluster we describe here is a possible aftershock sequence (on the CLSC), with the rest appearing as swarm activity — events clustered in time and space with no clear mainshock. Earthquake swarms described in the literature are typically linked to volcanic (Dziak and Fox, 1999; Tolstoy et al., 2006) or hydrothermal processes (Tolstoy et al., 2008; Wilcock et al., 2002). No swarms found here can be easily attributed to either of these driving mechanisms as they lie far from known hydrothermal sites and tend to be in locations with likely reduced magmatic activity (e.g., near segment ends). However, each of these features are associated with young, evolving, or ephemeral tectonics. For example, the nELSC has been actively retreating with advancement of the CLSC rift where twelve located events occurred within a five hour period (Fig. 5). Swarm activity dominates the Peggy Ridge extensional transform region where the southern portion of the transform is manifesting as an extensional reorganization of the prior PR strike–slip transform fault. In contrast, the northernmost portion has not reoriented into an extensional regime and does not exhibit time clustering behavior in seismicity (Fig. 4).

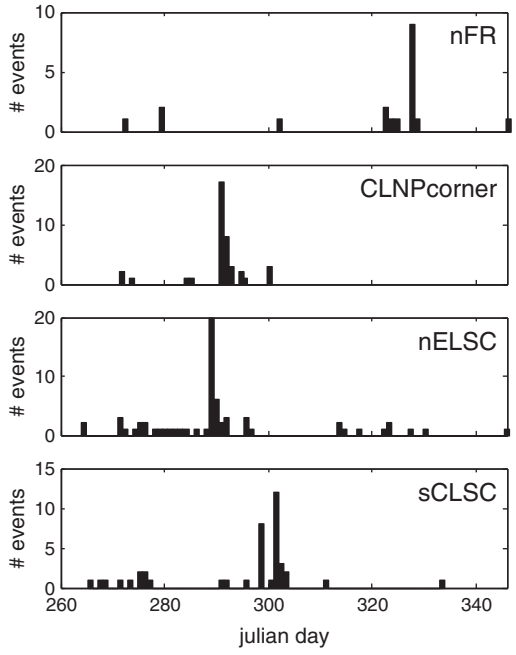

Fig. 5. Histograms of events in time. Panels show events within each region of clusters marked in Fig. 4. Excepted are clusters from the ETZ which are treated separately later. Clustering dominates over steady release in each of these regions.

4.1.2. ELSC

Most of the seismicity associated with the ELSC is found at the northern terminus,(nELSC), which has events recorded in the CMT and PDE catalogs. CMTs near the nELSC are predominantly strike–slip, consistent with bookshelf faulting at the step over between the CLSC and ELSC (Wetzel et al., 1993). As the ELSC retreats with CLSC propagation (Parson et al., 1990), this portion of the ridge can be viewed as a dying rift in that the locus of spreading is moving from the ELSC to the CLSC. However, it is not quite that simple, in that a nanoplate abutting the CLSC and ELSC exhibits some motion along the ELSC extension (see 4.1.6). Other than at the northern terminus, only three events are unambiguously identified as occurring along the length of the ELSC. These three are identified solely by T-waves, with two coming from virtually the same location within 4 min of each other.

The ELSC exhibits an excess degree of hydrothermal venting relative to the global spreading rate trend. Baker et al. (2006) and Martinez et al. (2006) suggest that the excess hydrothermal activity derives from increased tectonic faulting with decreased magma supply. Such a model suggests that small earthquakes will concentrate on the northernmost, magma-starved section of the ELSC, and there should be few earthquakes on the southern, magmatically robust section. Moreover, it depends on localized faulting to accommodate deformation that would have been accommodated by magmatic intrusion to enhance permeability. Despite the less than 20 km proximity to a hydrothermal site for each of three located events, they are likely tectonic rather than related to hydrothermal activity as the vent sites are outside the two sigma confidence ellipses.

The dearth of events suggests that ELSC seismicity tends to be small and/or infrequent. Recordings from an active source OBS array in 2009 shows that there is considerable seismic activity associated with the ELSC as measured by events per hour (Conder et al., 2009), but the small magnitudes require an OBS array tightly focused on the ELSC to adequately record and locate the events, consistent with a model of deformation accommodated primarily by magmatic extension.

4.1.3. CLSC/propagator

The Central Lau Spreading Center extends from ~18°S to ~19° 25′S where it is propagating southward at the expense of the ELSC (Parson et al., 1990). The CLSC shows seismicity along its length, with 47 located events, appearing to be the most seismically active spreading center in the basin. This may be due to sampling bias as the only spreading center that directly crosses the main line of the OBS array, allowing for a lower detection threshold than necessary for other spreading centers within the basin. With the southernmost tip actively propagating, there is likely a difference in the mode of tectonic deformation between the tip and the rest of the spreading center. Of the 47 located CLSC events, 39 lie south of 18° 54′S towards the ridge tip rather than the segment center. CLSC seismicity exhibits some clustered activity. Over half of the recorded events occurred over a seven day period (Fig. 5) containing a possible aftershock sequence giving it a slightly different character from the other clusters.

Unlike other tectonically evolving features in the basin, the propagating rift may not exhibit swarm activity. The difference may lie in mode of tectonic evolution. Abyssal hill morphology of the CLSC propagating rift is consistent with other propagating rifts that propagate in discrete jumps rather than through gradual processes (Wilson, 1990). This difference suggests that the propagating rift may be viewed as in a ‘meta-stable’ state and therefore may not spawn swarm activity like other actively evolving tectonic features.

4.1.4. Fonualei rift

Although the ridge axes do not generally exhibit as much seismicity as other crustal boundaries, clear seismicity is located along the Fonualei rift. We find more events associated with the northern terminus of the FR near the Mangatolu triple junction (MTJ) than with the rift tip despite CMT and PDE catalogs listing many more events near the rift tip than near the northern end. The northern terminus left-steps towards the MTJ in the form of a small overlapping spreading center (OSC) (Fig. 4), likely indicating an evolving plate boundary in this region (Perram and Macdonald, 1994; Ruellan et al., 1994). Likewise, single link clustering shows most of the activity near the terminus occurs in one swarm on the eastern flank of the OSC (Fig. 4), consistent with the evolving portions of the ridge responding seismically in a more time-dependent manner. The propagating tip at the southern end of the ridge may behave without swarm activity, like the CLSC propagator. However, the FR tip does not show an abyssal hill morphology similar to the CLSC and may be propagating in a more gradual fashion. As the tip has far more recorded seismicity from regional and global catalogs than the northern terminus, the dearth of events there lends credence to the possibility that it also exhibits swarm-like activity, but with the LABATTS deployment in an inopportune recording window.

4.1.5. Lau extensional transform zone

The single-most seismically active feature in the basin is the Lau extensional transform zone (ETZ). The high rate of seismicity was recognized in the 1980s by Eguchi et al. (1989), who recorded more than ten events per day along the ETZ with a thirty day, small aperture OBS deployment centered on the ETZ. We locate more than 600 events along the Peggy Ridge (PR) and ETZ (Figs. 4 and 6). In addition, station D005, near the northern end of the ETZ was triggered by the autopicking algorithms far more times than any other station, implying hundreds, if not thousands, of nearby events that we were unable to locate with the other instruments. S–P times show that these events are consistent with being derived from the ETZ. In separating out the southern events associated with the more extensional part of the ETZ from the more distinct PR transform in the northwest, we see that much of that activity in the southern section comes in a few energetic swarms, while events from the northwest part of the zone along the PR transform are steadier in their frequency of occurrence (Fig. 7).

Eguchi et al. (1989) grouped clusters of seismicity within the zone into six sections (A–F). As the LABATTS array is spread across the basin, we do not have the same resolution to tightly constrain the seismicity to the Eguchi clusters along the ETZ. However, the density of events along the ETZ, as evaluated by summing confidence ellipses of each event as a 2D Gaussian distribution, has a 'bumpiness' that is consistent with these discrete event clusters, albeit with some small shifts (Fig. 6). Intriguingly, we observe far less activity along Eguchi segments A–C (between 17° and 17° 30′S) and more near E–F (between 17° 35′ and 18°S), opposite in overall trend from the previous study, further demonstrating the non-steady state behavior of ETZ seismicity. The seismicity in each of the high density sections comes in punctuated swarms. The two high density sections equivalent to Eguchi E–F, are dominated by clusters of events in time, each lasting for roughly a day or two in duration. Curiously, swarms in these two clusters are often 1 day apart in either direction (Fig. 7), hinting of possible stress interaction between adjacent segments.

4.1.6. Nanoplate

Seismicity delineates a nanoplate (~1 order of magnitude smaller than other microplates) in the central basin bounded by the CLSC propagating rift to the west and by the CLSC/ELSC bookshelf faulting zone (Wetzel et al., 1993) to the south (Fig. 8). The nanoplate is

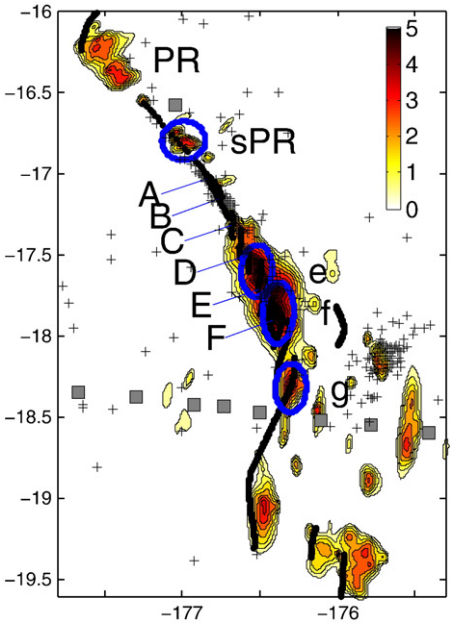

Fig. 6. Event density along Peggy Ridge (PR), extensional transform zone (ETZ), and central Lau nanoplate. More than 600 events were located along this feature. The two sigma confidence ellipses for each event are summed as Gaussian distributions. Color scale is density in log units. Event density is variable along the zone. Eguchi et al. (1989) found seven discrete loci of events, marked A–F, and what they termed 'isolated activity' east of the ETZ. Events from Eguchi et al. are marked as crosses. While they found more seismicity in regions A–C, we see far more activity further to the south and north. Blue ellipses mark regions of histograms shown in Fig. 7. For consistency with the previous work, we label the three southern groups 'e', 'f', and 'g'.

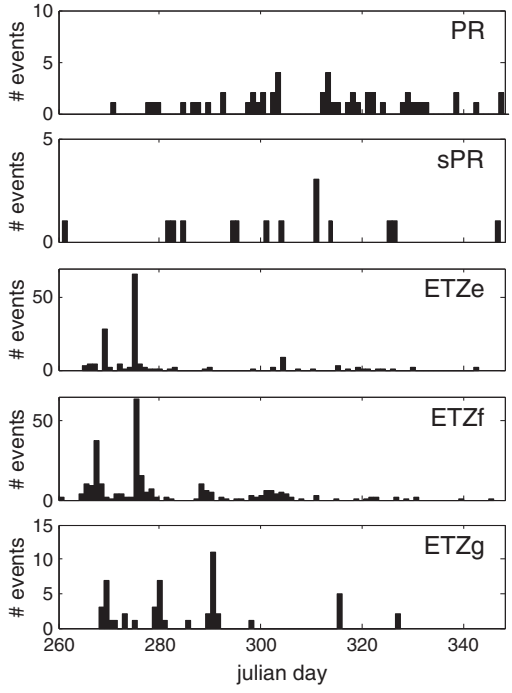

Fig. 7. Histograms of LETZ events. Five panels show regions within five ellipses marked in Fig. 6. PR and sPR are along the Peggy Ridge transform, while e, f, and g are well within the extensional part of the zone. Horizontal axis denotes julian day of the experiment, and vertical axis is binned number of events per day. Note different scales. PR and sPR have 56 and 15 located events, while e, f, and g have 172, 276, and 43 respectively. The southern groups are much more prone to swarm activity than the northern end of the transform. Event activity along PR and sPR are steadier in time where there has been little recent change in plate boundary geometry, while the southern groups tend to come in punctuated clusters. While coming from different loci, swarms are observed in each of the tree groups near days 270, 280, and 290, suggesting that swarms may trigger other swarms on adjacent segments.

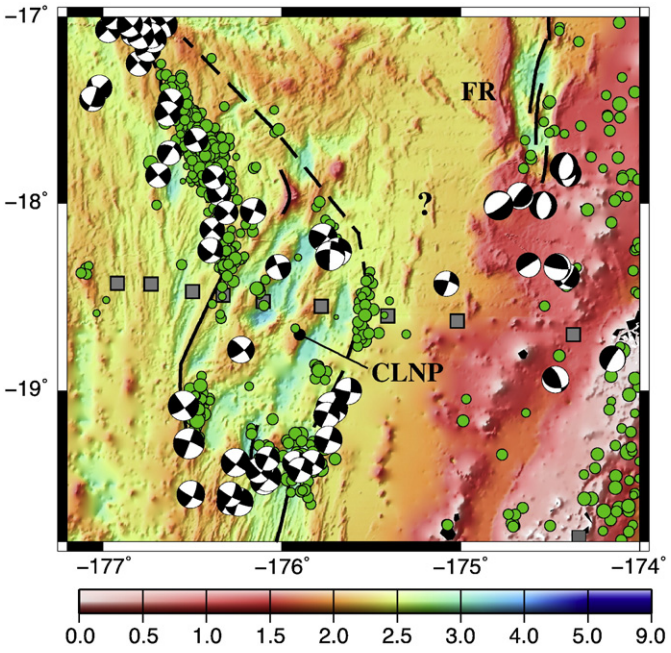

Fig. 8. Central Lau basin bathymetry and seismotectonics. Color bar denotes water depth in kilometers. Spreading system shown as solid black lines. Earthquakes located in this study density are shown as green circles. Shallow CMTs (≤25 km depth) from Harvard are shown. FR = Fonualei rift tip; CLNP = central Lau nanoplate; ? = region of predicted tectonic strain with notable lack of seismicity. Newly identified boundary of a nanoplate is shown as dashed.

bounded on the east roughly by the northward trending extension of the ELSC and to the north by the ESE trending extension of the ETZ. This nanoplate is likely an ephemeral feature and characterized by rough topography arising from overlapping spreading and ELSC decapitation as the CLSC has propagated southward, similar to microplate evolution observed on the EPR (Bird et al., 1999). The northeastern corner is also a locus of swarm activity found in the SLC analysis. Station W018, close to the event clustering, is second only to D005 in the number of P–S pairs found, but not associated with a specific event because of too few arrivals on other stations. The dynamics of this nanoplate are beyond the scope of this paper and will be covered in a manuscript to follow, but it shows similar morphological characteristics, such as a bounding propagating rift and complex seafloor morphology as observed at other rapidly evolving nanoplates and microplates (Goff et al., 1993; Naar and Hey, 1991). Despite the prominent seismicity along the eastern edge of the nanoplate, there is little indication of a narrow boundary in the bathymetry or sidescan sonar, suggesting that this may be better viewed as a boundary of somewhat diffuse deformation.

4.1.7. Microplate geometry

Contrary to expectations, crustal seismicity does not delineate a clear southern boundary for the hypothesized Niuafo'ou plate between the CLSC/ELSC and the Fonualei rift (Fig. 8). One event with a resolvable CMT occurred in this gap in 1996, possibly indicating this deformation, but remains unsupported by any shallow seismicity from this study. The lack of deformation extending from the Fonualei rift towards the nanoplate or ridge system where over 4.5 cm/yr of strain is predicted is still a puzzle. The tip is propagating southward towards the arc (Zellmer and Taylor, 2001), implying that the boundary is adjusting in location. It seems plausible that a migrating boundary may not localize enough to affect seafloor morphology, but the high degree of strain should result in some degree of seismic deformation.

The absence of crustal seismicity between the FR rift tip and nanoplate leads to two different possibilities for consideration. The first is that the N–T pole determined from FR data overpredicts the amount of deformation that needs to be accommodated between the FR and Lau ridge system. The Tonga–Niuafo'ou pole determined by Z&T lies near 20°S, more than 2° from the rift tip. Because the seafloor magnetization pattern is complex and poorly constrained along the FR axis, they limited their spreading rate measurements to two from the northern part of the axis near the MTJ. While the azimuth to the pole is well constrained, the calculated distance to the pole along that azimuth is entirely controlled by the ratio of these two measurements. We suggest that the pole is closer to the FR rift tip, nearer 18° 30′S, 174° 30′W with an increased opening rate of 17.4°/Myr. This shift in more than 1.5° of latitude only requires an error of 5% in one of the two rate measurements and reduces the amount of unaccounted for strain from 4.5 cm/yr to 1.8 cm/yr. If the rate measurements are overestimated because of influence from the OSC near the MTJ, the unaccounted for strain would be smaller still.

The other possibility is that there is no boundary extending between the FR and the CLSC. Rather, the boundary extends from the FR tip to the trench — possibly through one of the loci of more intense forearc seismicity. This alignment fixes the previously termed Niuafo'ou plate with the Tonga plate and results in the northeast corner of the basin acting as a separate Niuatoputapu plate, with the nanoplate couched against the CLSC explaining why the previous statistical analysis of plate boundary data indicated a triple junction at the southern end of the CLSC. The Tonga–Niuatoputapu pole would be constrained by spreading along the FR, and thus be the same as the already determined Niuafo'ou–Tonga pole. However, a Niuatoputapu model requires a spreading rate of <3 cm/yr along the Fonualei rift to satisfy geodetic constraints from the Tongan islands (Bevis et al., 1995). Given the several criteria that must be satisfied for a Niuatoputapu model, we lean towards the presently defined microplate geometry and shifting the N–T pole northward.

4.2. Northern basin

As the three-plate model applies to the basin south of ~16°S, the roughly 100 km wide region abutting the northernmost edge of the basin is unconstrained by the model. This region, as it is not part of the Niuafo'ou (or Tonga) microplate, must comprise one or more micro (nano)plates. Because this region is less well mapped than the central or southern basin, the geometry of crustal deformation boundaries along with their associated tectonics are largely left to inferences from seismicity. Our threshold for detection is higher in the northern basin than in the central basin, due to distance from the mainline of the array. Nonetheless, some useful pieces of information towards teasing out the northern basin tectonics can be gleaned from these results.

4.2.1. Microplate boundary near Niuafo'ou

The northern boundary of the Niuafo'ou microplate is delineated along the northwestern corner by the Northwest Lau Spreading Center (NWLSC) (Fig. 1), but it is not well established where the boundary traces between the NWLSC and the Mangatolu triple junction (MTJ) to the east. Seafloor reflectivity shows a rightward-stepping discontinuity from the NWLSC to another rift segment near 176° 45′W, 15° 35′S (Zellmer and Taylor, 2001). Beyond this, regional and global seismic catalogs broadly show deformation tracing eastward from roughly 176°W to the MTJ.

Pelletier et al. (1998) and Tiffin (1993) suggest the microplate boundary connects the NELSC and the NWLSC through an extensional, left-lateral transform zone, but did not have the resolution to give more detail about this boundary. Fortunately, shallow seismicity found in this study, in conjunction with the global catalogs, gives a few clues. For instance, a group of events near 15° 15′S, 176°W give a likely tie point of the boundary connecting the NWLSC with the MTJ.

These events trend ESE suggesting a right-stepping fault towards the island of Niuafo'ou (Fig. 9). Near Niuafo'ou, the boundary turns northeast for about 50 km before turning southeast towards the Mangatolu triple junction (Fig. 9), overall consistent with the suggested left-lateral zone of extension, although difficult to discern in the bathymetry.

4.2.2. Northwest Lau triple junction

Shallow seismicity exhibits a well-defined line of seismicity extending NNW from the southernmost segment of the NWLSC (Fig. 9), rather than right-stepping towards the next segment. Recently collected bathymetry and reflectivity confirm the location of the right-stepped segment with a connecting non-transform discontinuity (Martinez and Taylor, 2006). This pattern of right-stepping axis geometry coupled with left-stepping earthquake epicenters suggests that this is a triple junction of a ridge — fault — non-transform discontinuity variety. For the given geometry, the newly found fault must be right lateral with a strain rate similar to the non-transform discontinuity to satisfy closure. Triple junction stability analysis (Cox and Hart, 1991) shows that this triple junction is likely stable, but shortening the ridge segment with time.

4.2.3. Network of small plates

An implication of the existence of this northwest Lau triple junction is that there must be at least two tectonic plates in the northern basin and hints at the likelihood of a greater number of micro (or nano) plates in the northern basin as has been previously supposed. It is possible that the northern basin between the northwest Lau triple junction and the MTJ to the east is not limited to one microplate, but partitioned into several. The shallow earthquakes trend northward near 175° 05′W in a region with a significant number of events recorded teleseismically (Fig. 9). It is possible that these events are deriving from the boundary of a nanoplate abutting the NELSC and MTJ. Given the trends in recorded seismicity elsewhere in the northern basin, it seems reasonable that another small plate or two remain to be identified, but will require more detailed geophysical mapping.

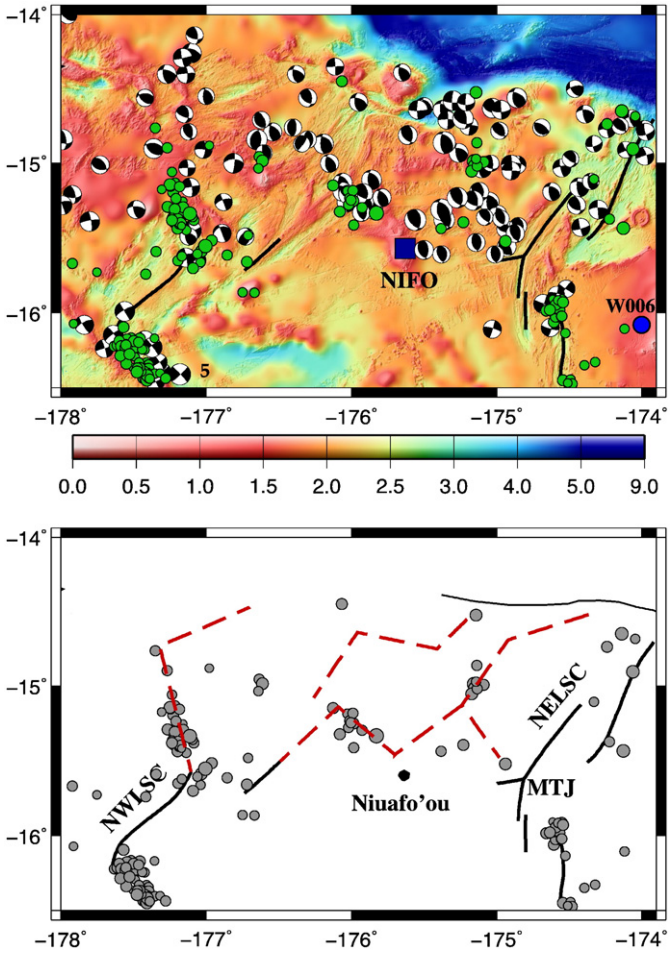

Fig. 9. Northern Lau basin. Top panel shows bathymetry and earthquakes. Symbols are same as Figs. 1 and 8. Bottom panel shows microplate boundaries in northern basin (dashed) as proposed on the basis of seismicity recorded locally and teleseismically. Given the observed patterns of seismicity, there is reasonable likelihood that the northern basin will be divided further with more detailed geophysical mapping of the region.

4.3. Arc volcanoes

More than a dozen different submarine volcanoes in the Tongan arc are known to have historical eruptions, including five in the last decade (Venzke et al., 2002). Of note, West Mata, in the northeastern basin, is a RIDGE2000 rapid response site (RIDGE2000 Science Plan, 2011) since discovery of active eruptions in 2008 (Merle et al., 2009). Underwater and island volcanoes can emit seismic waves during episodes of magmatism (e.g., Dziak and Fox, 1999). While volcanic events are notably few in the present dataset, a handful of earthquakes are closely located with specific arc volcanoes, such as Metis Shoal at 19° 12′S which erupted in 1995 and an unnamed seamount at 18° 20′S which erupted in 2001 (Venzke et al., 2002), possibly indicating precursors to these eruptions. Other volcanic signals, such as magmatic tremor, are possibly recorded in the LABATTS data on individual stations, such as station W006 near the northern end of the volcanic line and W007 in the northwest basin (Fig. 1), both of which show a considerable degree of nonimpulsive signal, sometimes lasting hours or longer. However, without independent confirmation from additional stations their connection to volcanic processes remains speculative and must wait further deployments for comparison.

5. Conclusions

Shallow basin seismicity often excites T-waves which are regularly seen at greater epicentral distances than body waves. With these arrivals, nearly a thousand shallow microseismic events are found in the backarc basin during the three month LABATTS OBS deployment. Notable loci of activity are observed, including a previously unrecognized triple junction in the northwest basin, a nanoplate in the central basin, and the ETZ, the most seismically active basin feature with more than 600 located events in the three month period.

The observed patterns of shallow seismicity build on and revise previously understood tectonics of the basin. The northern basin likely comprises a network of small tectonic plates. A newly found triple junction in the northwestern basin is part of this network (Fig. 9), but more detailed systematic geophysical mapping is necessary in the northernmost basin to fully constrain their geometries and kinematics. A nanoplate is found in the central basin, bounded by the CLSC to the west, the ELSC/CLSC non-transform discontinuity to the south and the southeast extension of the Peggy Ridge transform to the north (Fig. 9).

Even with the greater fidelity provided by the ocean bottom seismograph experiment, there is still no indication of plate boundary deformation connecting the Fonualei rift to the Lau ridge system. To account for the lack of observed deformation, we suggest a revised Niuafo'ou–Tonga pole that predicts <2 cm/yr of strain in this region. Geodetic constraints coupled with improved spreading rate data from the Fonualei rift can test this possibility.

The abundance of swarm activity in the basin is unlikely to be driven by magmatic or hydrothermal activity. Rather, they appear to be associated with regions exhibiting active reorganization or other time-dependent tectonics. Actively changing plate boundaries dominated by swarm activity include the ETZ, the northern termini of the ELSC and FR, and nearly the entire perimeter of the CLNP, while more

stable features show little time dependence at least at this multi-monthly scale.

Acknowledgements

We thank Dylan Matthieu and Simon Heath for their work in transferring and reformatting the data. Thanks to Fernando Martinez for sharing shipboard geophysical data near the NWLSC prior to publication. Brian Taylor and an anonymous reviewer provided thoughtful critical comments that greatly improved the quality of the manuscript. This work was funded by NSF grants OCE-0825424 and OCE-0426408.

References

Baker, E.T., Resing, J.A., Walker, S.L., Martinez, F., Taylor, B., Nakamura, K.-I., 2006. Abundant hydrothermal venting along melt-rich and melt-free ridge segments in the Lau back-arc basin. Geophys. Res. Lett. 33.

Bevis, M., Taylor, F., Schutz, B., Recy, J., Isacks, B., Helu, S., Singh, R., Kendrick, E., Stowell, J., Taylor, B., Calmant, S., 1995. Geodetic observations of very rapid convergence and back-arc extension at the Tonga arc. Nature 374, 249–251.

Bird, R., Tebbens, S., Kleinrock, M., Naar, D., 1999. Episodic triple-junction migration by rift propagation and microplates. Geology 27, 911–914.

Conder, J., Wiens, D., 2006. Seismic structure beneath the Tonga arc and Lau back-arc basin determined from joint Vp, Vp/Vs tomography. Geochem. Geophys. Geosyst. 7, Q03018.

Conder, J.A., Dunn, R., Godfrey, K., 2009. Preliminary examination of microearthquake activity along the Eastern Lau Spreading Center and southern Lau Basin. EOS, Trans AGU 90, Abstract OS13A-1161.

Cox, A., Hart, B.R., 1991. Plate Tectonics: How It Works. Wiley-Blackwell.

Crawford, W., Hildebrand, J., Dorman, L., Webb, S., Wiens, D., 2003. Tonga Ridge and Lau Basin crustal structure from seismic refraction data. J. Geophys. Res. 108, 2195.

Davis, S., Frohlich, C., 1991. Single-link cluster analysis, synthetic earthquake catalogs, and aftershock identification. Geophys. J. Int. 104, 289–306.

Dunn, R., 2009. Crustal Accretion and Mantle Processes along the Subduction Influenced Eastern Lau Spreading Center. L-SCAN, Project.

Dziak, R.P., 2001. Empirical relationship of T-wave energy and fault parameters of northeast Pacific Ocean earthquakes. Geophys. Res. Lett. 28, 2537–2540.

Dziak, R.P., Fox, C.G., 1999. The January 1998 earthquake swarm at axial volcano, Juan de Fuca ridge: hydroacoustic evidence of seafloor volcanic activity. Geophys. Res. Lett. 26, 3429–3432.

Dziak, R.P., Smith, D.K., Bohnenstiehl, D.R., Fox, C.G., Desbruyeres, D., Matsumoto, H., Tolstoy, M., Fornari, D.J., 2004. Evidence of a recent magma dike intrusion at the slow spreading Lucky Strike segment, Mid-Atlantic Ridge. J. Geophys. Res. B Solid Earth 109, 1–15.

Eguchi, T., Fujinawa, Y., Ukawa, M., 1989. Microearthquakes and tectonics in an active back-arc basin; the Lau Basin. Phys. Earth Planet. Int. 56, 210–229.

Fox, C., Matsumoto, H., Lau, T., 2001. Monitoring Pacific Ocean seismicity from an autonomous hydrophone array. J. Geophys. Res. 106, 4183–4206.

Goff, J., Fornari, D., Cochran, J., Keeley, C., Malinverno, A., 1993. Wilkes transform system and nannoplate. Geology 21, 623–626.

Gudmundsson, O., Sambridge, M., 1998. A regionalized upper mantle (RUM) seismic model. J. Geophys. Res. 103, 7121–7136.

Hamburger, M.W., Isacks, B.L., 1988. Diffuse back-arc deformation in the southwestern Pacific. Nature 332, 599–604.

Hojstrup, J., 1993. A statistical data screening procedure. Meas. Sci. Technol. 4, 153–157.

Igarashi, T., Matsuzawa, T., Umino, N., Hasegawa, A., 2001. Spatial distribution of focal mechanisms for interplate and intraplate earthquakes associated with the subducting Pacific plate beneath the northeastern Japan arc: a triple-planed deep seismic zone. J. Geophys. Res. 106, 2177–2191.

Isacks, B.L., Sykes, L.R., Oliver, J., 1968. Distribution in time of small deep and shallow earthquakes in the Fiji–Tonga region. Spec. Pap. Geol. Soc. Am. 101, 315.

Knapmeyer, M., 2004. TTbox: a Matlab toolbox for the computation of 1D teleseismic travel times. Seis. Res. Lett. 75, 726–733.

Koper, K.D., Wiens, D.A., Dorman, L.M., Hildebrand, J.A., Webb, S.C., 1998. Modeling the Tonga Slab; can travel time data resolve a metastable olivine wedge? J. Geophys. Res. 103, 30,079–30,100.

Martinez, F., Taylor, B., 2006. Modes of crustal accretion in back-arc basins: inferences from the Lau basin. In: Christie, Fisher, Lee, Givens (Eds.), Back-Arc Spreading Systems — Geological, Biological, Chemical, and Physical Interactions: AGU Monogr., 166, pp. 5–30.

Martinez, F., Taylor, B., Baker, E.T., Resing, J.A., Walker, S.L., 2006. Opposing trends in crustal thickness and spreading rate along the back-arc Eastern Lau Spreading Center: implications for controls on ridge morphology, faulting, and hydrothermal activity. Earth Planet. Sci. Lett. 245, 655–672.

Merle, S.R., J.A., Embley, R.W., Collasius, T.R., J.A., Embley, R.W., Collasius, T., 2009. Northeast Lau Basin Response Cruise (NELRC) R/V Thomas G. Thompson Expedition TN-234, Cruise Report.

Naar, D.F., Hey, R.N., 1991. Tectonic evolution of the Easter microplate. J. Geophys. Res. 96, 7961–7993.

Park, M., Odom, R.I., Soukup, D.J., 2001. Modal scattering a key to understanding oceanic T-waves. Geophys. Res. Lett. 28, 3401–3404.

Parson, L., Pearce, J., Murton, B., Hodkinson, R., 1990. Role of ridge jumps and ridge propagation in the tectonic evolution of the Lau back-arc basin, Southwest Pacific. Geology 18, 470–473.

Pelletier, B., Louat, R., 1989. Seismotectonics and present-day relative plate motions in the Tonga–Lau and Kermadec–Havre region. Tectonophysics 165, 237–250.

Pelletier, B., Calmant, S., Pillet, R., 1998. Current tectonics of the Tonga–New Hebrides region. Earth Planet. Sci. Lett. 164, 263–276.

Perram, L., Macdonald, K., 1994. An overlapping propagating spreading center at 87 30′ W on the Galapagos spreading center. Earth Planet. Sci. Lett. 121, 195–211.

RIDGE2000 Science Plan, http://www.ridge2000.org/science/info/science_plan.php, accessed, January, 2011.

Roth, E.G., Wiens, D.A., Dorman, L.M., Hildebrand, J., Webb, S.C., 1999. Seismic attenuation tomography of the Tonga–Fiji region using phase pair methods. J. Geophys. Res. 104, 4795–4810.

Ruellan, E., Huchon, P., Auzende, J., Gracia, E., 1994. Propagating rift and overlapping spreading center in the north Fiji basin. Mar. Geol. 116, 37–56.

Smith, D., Escartin, J., Cannat, M., Tolstoy, M., Fox, C., Bohnenstiehl, D., Bazin, S., 2003. Spatial and temporal distribution of seismicity along the northern Mid-Atlantic Ridge, (15 degrees–35 degrees N). J. Geophys. Res. 108.

Taylor, B., Zellmer, K., Martinez, F., Goodliffe, A., 1996. Sea-floor spreading in the Lau back-arc basin. Earth Planet. Sci. Lett. 144, 35–40.

Tiffin, D., 1993. Tectonic and structural features of the Pacific Indo-Australian plate boundary in the north Fiji–Lau basin regions, Southwest Pacific. Geo-Mar. Lett. 13, 126–131.

Tolstoy, M., Cowen, J., Baker, E., Fornari, D., Rubin, K., Shank, T., Waldhauser, F., Bohnenstiehl, D., Forsyth, D., Holmes, R., Love, B., Perfit, M., Weekly, R., Soule, S., Glazer, B., 2006. A sea-floor spreading event captured by seismometers. Science 314 (5807), 1920–1922.

Tolstoy, M., Waldhauser, F., Bohnenstiehl, D., Weekly, R., Kim, W., 2008. Seismic identification of along-axis hydrothermal flow on the East Pacific Rise. Nature 451 (7175), 181–U187.

Venzke, E., Wunderman, R.W., McClelland, L., Simkin, T., Luhr, J., Siebert, L., Mayberry, G., Sennert, S., 2010. Global Volcanism, 1968 to the Present, Global Volcanism Program Digital Information Series. Smithsonian Institution. http://www.volcano.si.edu/. accessed.

Wetzel, L.R., Wiens, D.A., Kleinrock, M.C., 1993. Evidence from earthquakes for bookshelf faulting at large non-transform ridge offsets. Nature 362, 235–237.

Wiens, D.A., Shore, P.J., McGuire, J.J., Roth, E., 1995. The Southwest Pacific Seismic Experiment. IRIS Newslett. 14, 1–4.

Wilcock, W.S.D., Archer, S.D., Purdy, G.M., 2002. Microearthquakes on the Endeavour segment of the Juan de Fuca Ridge. J. Geophys. Res. B Solid Earth 107.

Willeman, R., 2001. Criteria for evaluating alternative hypocentres, analysis paper. Int. Seismological Center.

Wilson, D., 1990. Kinematics of overlapping rift propagation with cyclic rift failure. Earth Planet. Sci. Lett. 96, 384–392.

Yang, Y., Forsyth, D., 2003. Improving epicentral and magnitude estimation of earthquakes from T phases by considering the excitation function. BSSA 93, 2106–2122.

Zellmer, K.E., Taylor, B., 2001. A three-plate kinematic model for Lau Basin opening. Geochem. Geophys. Geosys. 2.